

Quantum dynamics of the femtosecond photoisomerization of retinal in bacteriorhodopsin

M. Ben-Nun,^{ab} Ferenc Molnar,^a Hui Lu,^{ac} James C. Phillips,^{ad} Todd J. Martínez^{ab} and Klaus Schulten^{abd}

^a Beckman Institute for Advanced Science and Technology, University of Illinois at Urbana-Champaign, Urbana, IL 61801, USA

^b Department of Chemistry, University of Illinois at Urbana-Champaign, Urbana, IL 61801, USA

^c Department of Nuclear Engineering, University of Illinois at Urbana-Champaign, Urbana, IL 61801, USA

^d Department of Physics, University of Illinois at Urbana-Champaign, Urbana, IL 61801, USA

The membrane protein bacteriorhodopsin contains all-*trans*-retinal in a binding site lined by amino acid side groups and water molecules that guide the photodynamics of retinal. Upon absorption of light, retinal undergoes a subpicosecond all-*trans* → 13-*cis* phototransformation involving torsion around a double bond. The main reaction product triggers later events in the protein that induce pumping of a proton through bacteriorhodopsin. Quantum-chemical calculations suggest that three coupled electronic states, the ground state and two closely lying excited states, are involved in the motion along the torsional reaction coordinate ϕ . The evolution of the protein–retinal system on these three electronic surfaces has been modelled using the multiple spawning method for non-adiabatic dynamics. We find that, although most of the population transfer occurs on a timescale of 300 fs, some population transfer occurs on a longer timescale, occasionally extending well beyond 1 ps.

Introduction

Bacteriorhodopsin (bR) is a protein which realizes the simplest known form of biological photosynthetic energy storage, absorbing light and converting its energy into a proton gradient across the cellular membrane of archaeobacteria through vectorial proton translocation.¹ bR, as its name indicates, is closely related to rhodopsin, the protein which acts as the primary light detector in the visual pathway of higher life forms. Recent reviews which discuss structure, function and spectroscopic properties of bR are given in ref. 2–6.

Bacteriorhodopsin has been an ideal system for investigations by physical chemists seeking information about the protein's dynamics and function, for three main reasons: The protein is unusually stable, it exhibits strong spectral shifts in the 400–600 nm range which are nearly uniquely connected to reaction intermediates,⁵ and it is possible to measure its time-dependent vibrational spectra, characterizing geometries as well as protonation states.² A high-resolution structure of bR, a prerequisite for a true understanding of the mechanism by which the protein couples its initial photoreaction to proton transport, first became available through the work of Henderson and co-workers.^{7,8} More recently, two other groups have reported more detailed structures.^{9,10}

The current structures reveal a pathway for the conduction of protons through the protein, lined with water molecules, in accord with previous predictions of molecular modelling.¹¹

In order to solve the riddle of the proton pump mechanism of bR, *i.e.* how proton transport is coupled to light absorption, one must focus on the photodynamics of the retinal chromophore which intercepts the proton conduction pathway. At the beginning of the photocycle, retinal is bound to the protein in an all-*trans* isomeric state through a Schiff base (C=N) linkage to a lysine side chain. It has been shown that the protonated Schiff base is directly involved in the proton translocation. After the initial photoprocess, and a series of spectroscopically well characterized intermediate states, the Schiff base proton is eventually transferred to the Asp85 side group of bR (to be later replenished from the Asp96 side group). The arrangement of the mentioned constituents, as shown in Fig. 1, is consistent with proton pumping in bR which, under native conditions, occurs from the cytoplasmic side to the extracellular side.

The key missing link for understanding the proton pump mechanism of bR is the exact nature of the photoproduct which triggers both proton release from retinal to Asp85 (the latter being connected to the extracellular side through a water channel), and

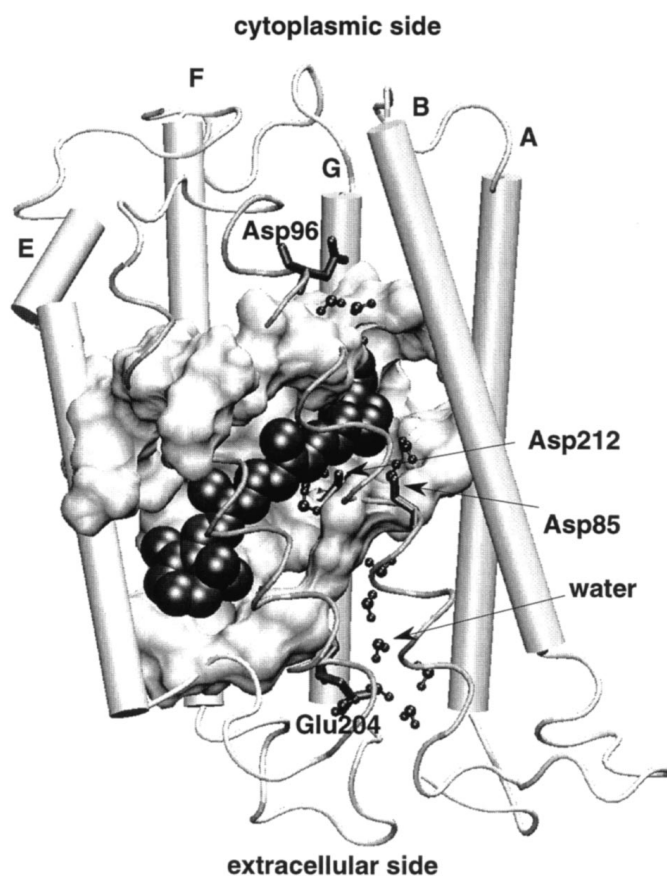


Fig. 1 bR and retinal binding site. Retinal is shown in van der Waals sphere representation, and part of nearby residues are shown in surface representation. Transmembrane helices A, B, E, F, G are shown as cylinders, and helices C, D are shown as thin tubes to reveal the retinal binding site. Note that the rendering of the retinal, for the sake of clarity, does not show hydrogen atoms; as a result retinal appears less voluminous than in reality. This figure was created with VMD.⁵⁸

a switch of retinal's Schiff base to a state in which the C=N group is protonated from Asp96 (in contact with the cytoplasmic side). Vibrational spectra of retinal reveal that it photoisomerizes around its $C_{13}=C_{14}$ bond (see Fig. 2 for an identification of this bond in retinal). Optical spectroscopy has also demonstrated that the initial photoisomerization proceeds within *ca.* 600 fs and is followed by a relaxation period of 2–3 ps. After this relaxation, the first intermediate that can be stabilized under low-temperature conditions is formed.^{12,13} Because of its ultrafast nature, the photodynamics connecting all-*trans*- and 13-*cis*-retinal constitutes an elementary physical process. Furthermore, the role of the protein is to provide a unique cavity (see Fig. 1) which stabilizes the product state. One expects that the molecular structure of the first intermediate state will reveal the pump mechanism; however, identification of this state at the level of detail relevant for the control of proton transfer reactions poses a great challenge.

Theoretical chemistry may meet this challenge before experiment does. Molecular dynamics simulations, in principle, can extrapolate the dynamics of bR from the initial state, provided through X-ray diffraction and electron microscopy,^{8–10} and can also master the short timescale of the photoreaction of bR. However, two obstacles must be overcome for such simulations to be accurate. First, one requires a faithful description of the potential-energy surfaces (PESs) governing the photoisomerization of retinal. Second, a suitable algorithm for describing the photoreaction on multiple-coupled PESs must be applied. These difficulties are compounded by the fact that the protonated Schiff base of retinal has two closely spaced excited states. The excited states stem from the well known low-lying optically forbidden 1A_g state and the optically allowed 1B_u state in polyenes.^{14,15} Although the ordering of these states is expected to switch in protonated Schiff base polyenes like retinal,¹⁶ nevertheless, they remain close. The higher-energy state, characterized by its predominant doubly excited character, is expected to lower its energy upon rotation around a double bond in bR. Thus, one expects three electronic states and at least two level crossings to play a role in the photodynamics (see Fig. 3).

In earlier studies, a mean-field approach (density matrix evolution¹⁷) was used to approximate the photoreaction dynamics on multiple PESs.¹⁸ However, the approximations involved in these calculations are known to fail when widely differing outcomes

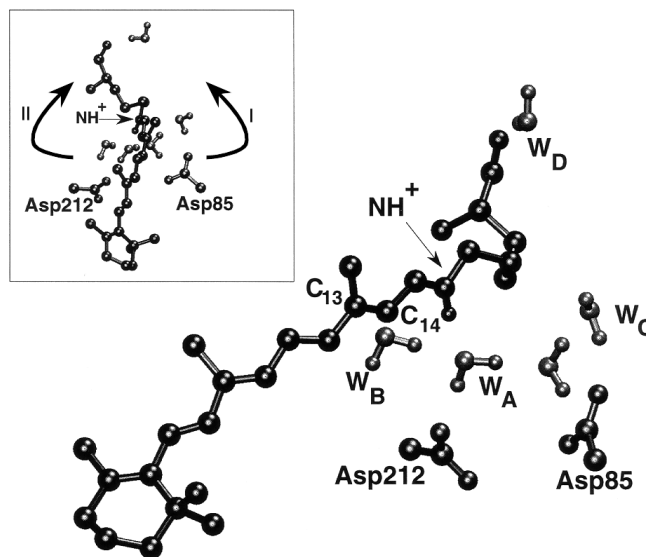


Fig. 2 Retinal binding site of bR. Retinal, Asp85, Asp212 and five nearby waters are drawn as CPK models. The inset shows a side view and distinguishes two directions for retinal isomerization: towards Asp85 (I) and towards Asp212 (II). This figure was created with VMD.⁵⁸

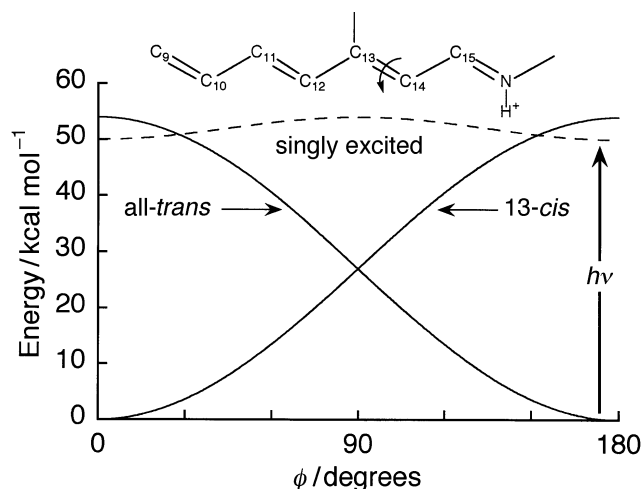


Fig. 3 The three diabatic PESs assumed in the computation as a function of the torsion angle of the $C_{13}=C_{14}$ bond. (---) Singly excited electronic state, (—) the (product) 13-*cis* ($\phi = 0^\circ$) and (reactant) all-*trans* ($\phi = 180^\circ$) electronic states. The minimum of the singly excited electronic state is matched to the measured excitation energy of bR. The arrow indicates the electronic excitation and the inset illustrates part of the retinal backbone.

are possible, such as isomerization in different directions (*vide infra*). In this contribution, a formally exact quantum-mechanical procedure (the full multiple spawning method) is used to study the *in situ* photodynamics of retinal. The results reveal how the geometry of the binding site of retinal in bR, together with the topology of retinal's electronic potential surfaces, can steer the photodynamics of retinal towards the key reaction product which triggers proton pumping. Though suggestive of a particular mechanism, the results should be considered as preliminary, in view of limitations in the resolution of the structure of bR available for the present study, and the need for further improvements of electronic energy surfaces and non-adiabatic couplings used in the simulations. The present paper provides a framework for future studies of the photodynamics of retinal in bR and of other biological photoprocesses, *e.g.* in photoactive yellow protein.¹⁹

Theory

The primary all-*trans* \rightarrow 13-*cis* phototransformation of bacteriorhodopsin proceeds on three coupled electronic states. The fact that these electronic states are coupled implies the breakdown of the Born–Oppenheimer approximation. Hence, straightforward solution of Newton's equations of motion is inappropriate. Instead, the quantum-mechanical nature of the nuclear degrees of freedom must be confronted. We, therefore, begin with a short review of non-adiabatic dynamics using the time-dependent quantum-mechanical approach.²⁰

Consider the time-dependent Schrödinger equation for a two electronic state system:

$$i \frac{\partial}{\partial t} \begin{pmatrix} \Psi_g \\ \Psi_e \end{pmatrix} = \begin{pmatrix} \hat{H}_g & \hat{V}_{ge} \\ \hat{V}_{eg} & \hat{H}_e \end{pmatrix} \begin{pmatrix} \Psi_g \\ \Psi_e \end{pmatrix} \quad (1)$$

where $\Psi_{g/e}$ is the projection of the wavefunction onto the ground/excited electronic state. (Atomic units are used in this paper, *i.e.* $\hbar = m_e = 1$.) The ground/excited state Hamiltonian, $\hat{H}_{g/e}$, is the sum of the kinetic and potential energy operators, and \hat{V}_{ge} represents the non-adiabatic coupling between the two PESs. Typically, only the ground electronic

state is populated initially, *i.e.* $\langle \Psi_g | \Psi_g \rangle = 1$ and $\langle \Psi_e | \Psi_e \rangle = 0$ at $t = 0$. Since the non-adiabatic coupling is usually spatially localized, the ground-state wavefunction will evolve according to the Hamiltonian \hat{H}_g [$\hat{H}_g = \hat{T} + \hat{V}_g(\mathbf{R})$] as long as the system is distant from a non-adiabatic region. During such time periods, the population on both states will remain constant. However, once the ground-state wavefunction approaches the non-adiabatic region, population will be transferred to the excited electronic surface and the wavefunction will bifurcate: one part of it will continue to evolve on the ground electronic state whereas the other part will evolve on the excited electronic state. During the non-adiabatic event, the motion of the ground and excited state wavefunctions will be correlated and population may cycle between the two states (*i.e.* Rabi oscillations). Once the non-adiabatic region has been traversed, and provided that neither the ground nor the excited state wavefunctions are trapped in this region, the coupling between the two components of the wavefunction will decrease to zero. Apart from a phase relation, both branches will continue to evolve independently under a well defined PES, *i.e.* $\hat{V}_g(\mathbf{R})$ for motion on the ground-state potential and $\hat{V}_e(\mathbf{R})$ for motion on the excited-state potential.

From this short discussion, it is apparent that the modelling of dynamics on multiple-coupled electronic states is straightforward in the context of a full numerical solution of the Schrödinger equation. However, because of the exponential scaling of computational effort with the number of degrees of freedom, an exact integration of the Schrödinger equation is practically impossible for large systems, *e.g.* for bR. For realistic large-scale simulations, numerically less demanding procedures must be developed. The full multiple spawning (FMS) method is an example of such a procedure.^{21–25} Other methods which have been advanced to model non-adiabatic dynamics include surface-hopping procedures,^{26–28} path-integral-based methods,^{29–31} and mean-field^{17,32} and related approximations.^{33,34} The relative merits of these approximations have been discussed previously.^{21,22,24} The FMS method has been used previously in studies of electronic quenching,^{24,35,36} photodissociation^{37,38} and pump-probe^{39,40} spectroscopy. It has been shown to provide a quantitatively accurate description of non-adiabatic dynamics in multi-dimensional non-adiabatic problems,²⁵ and its relationship to classical mechanics has been discussed.²²

The FMS method uses a time-dependent basis set for the wavefunction. The key idea behind the method is to expand the size of the basis only during non-adiabatic events, using the available information to predict the regions of phase space where population will be created. This dynamical expansion of the number of basis functions is accomplished *via* a spawning procedure, which keeps the basis size manageable while ensuring that it provides a reasonable approximation to the exact wavefunction. Because classical mechanics serves as a guide for basis set propagation (and selection), the computational effort remains classical-like (and existing molecular dynamics programs can be employed) yet quantum-mechanical electronic state-changing effects are included. The method has previously been discussed in detail (see ref. 24 and 25) and we review it only briefly in what follows.

The general multi-electronic state Hamiltonian operator can be written as

$$\hat{H} = \sum_I |I\rangle \hat{H}_{II} \langle I| + \sum_{I' \neq I} |I\rangle \hat{H}_{II'} \langle I'| \quad (2)$$

where, unlike in eqn. (1), the electronic states I are denoted in bra-ket notation. As in eqn. (1), the electronic states are taken to be orthonormal and the operators \hat{H}_{II} and $\hat{H}_{II'}$ act only on the nuclear degrees of freedom. The FMS method uses a multi-configurational frozen Gaussian nuclear wavefunction ansatz of the form

$$\Psi = \sum_I C_I(t) \chi_I(\mathbf{R}; t) |I\rangle \quad (3)$$

which can be applied for any number of electronic states and nuclear degrees of freedom. Here, the wavefunction, Ψ , is expressed as a weighted sum over electronic states of normalized wavefunctions. Every component in this sum is a product of an electronic wavefunction (*i.e.* allowed to depend parametrically on the nuclear coordinates) and a time-dependent nuclear wavefunction. Since each electronic state has its own nuclear wavefunction, one has direct access to dynamical quantities on each electronic state. Each of the time-dependent nuclear wavefunctions, $\chi_I(\mathbf{R}; t)$, is represented as a linear combination of multi-dimensional Gaussian basis functions⁴¹ with time-dependent amplitudes

$$\chi_I(\mathbf{R}; t) = \sum_j d_{I,j}(t) \chi_j^I(\mathbf{R}; \bar{\mathbf{R}}_j^I(t), \bar{\mathbf{P}}_j^I(t), \bar{\gamma}_j^I(t), \alpha_j^I) \quad (4)$$

where the indices I and j label the j th nuclear basis function on electronic state I , and all the time dependence of the basis functions is explicitly denoted. For multi-dimensional problems, it is most convenient to use a Cartesian coordinate system and construct each of the multi-dimensional Gaussian basis-functions in eqn. (4) as a product of $3N$ one-dimensional Gaussian functions

$$\chi_j^I(\mathbf{R}; \bar{\mathbf{R}}_j^I(t), \bar{\mathbf{P}}_j^I(t), \bar{\gamma}_j^I(t), \alpha_j^I) = \exp[i\bar{\gamma}_j^I(t)] \prod_{\rho}^{3N} \tilde{\chi}_j^I(\mathbf{R}; \bar{R}_{\rho j}^I(t), \bar{P}_{\rho j}^I(t), \alpha_j^I) \quad (5)$$

$$\tilde{\chi}_j^I(\mathbf{R}_{\rho}; \bar{R}_{\rho j}^I(t), \bar{P}_{\rho j}^I(t), \alpha_j^I)$$

$$= \left(\frac{2\alpha_{\rho j}^I}{\pi} \right)^{1/4} \times \exp\{-\alpha_{\rho j}^I [R_{\rho} - \bar{R}_{\rho j}^I(t)]^2 + i\bar{P}_{\rho j}^I(t) [R_{\rho} - \bar{R}_{\rho j}^I(t)]\} \quad (6)$$

where the index ρ , $\rho = 1, 2, \dots, 3N$ enumerates the $3N$ Cartesian coordinates for a system with N atoms. The time evolution of the parameters in each Gaussian is described according to Hamilton's equations of motion, so that each Gaussian state is centred along a classical trajectory governed by

$$\dot{\bar{R}}_{\rho j}^I(t) = \bar{P}_{\rho j}^I(t) / M_{\rho} \quad (7)$$

$$\dot{\bar{P}}_{\rho j}^I(t) = -\partial V_I(\mathbf{R}) / \partial R_{\rho j} \Big|_{\bar{\mathbf{R}}_j^I(t)} \quad (8)$$

The propagation of the nuclear phase $\bar{\gamma}_j^I(t)$ is described by

$$\dot{\bar{\gamma}}_j^I(t) = \sum_{\rho}^{3N} \frac{1}{2M_{\rho}} \{[\bar{P}_{\rho j}^I(t)]^2 - 2\alpha_{\rho j}^I\} - V_I[\bar{\mathbf{R}}_j^I(t)] \quad (9)$$

which involves the classical Lagrangian as well as a contribution from the width of the Gaussian state. In eqn. (7)–(9), M_{ρ} is the mass of the ρ th atom, $V_I(\mathbf{R})$ is the potential energy for state I , and the overdot denotes a time derivative. Note that a single nuclear phase factor, $\bar{\gamma}_j^I(t)$, is associated with each multi-dimensional Gaussian [*cf.* eqn. (5)]. In general, the time-independent width that is associated with each Gaussian, $\alpha_{\rho j}^I$, should be viewed as a parameter chosen heuristically; it has been previously found that, for suitable ranges of parameter values, the results are independent of its specific value.

Given the orthonormality of the electronic states, the remaining equations of motion for the quantal amplitudes for being in the nuclear basis state j on the electronic state I at time t , $D_j^I(t) = C_I(t) d_{I,j}(t)$, are given by the time-dependent variational principle^{22,24,41} [or equivalently by substituting the wavefunction ansatz of eqn. (3)–(5) into the time-dependent Schrödinger equation] as

$$\dot{\mathbf{D}}^I = -i(\mathbf{S}_I)^{-1} \left\{ [\mathbf{H}_{II} - i\dot{\mathbf{S}}_I] \mathbf{D}^I + \sum_{I' \neq I} \mathbf{H}_{II'} \mathbf{D}^{I'} \right\} \quad (10)$$

where \mathbf{S}_I is the time-dependent overlap matrix of the Gaussian basis functions on electronic surface I , $\mathbf{H}_{II'}$ is the sub-block of the Hamiltonian matrix describing the interaction between basis functions on electronic state I and I' and $\dot{\mathbf{S}}_I$ is the matrix representation of the right-acting time-derivative operator, *i.e.*

$$(\mathbf{D}^I)_j \equiv C_I d_j^I \quad (11)$$

$$(\mathbf{S}_I)_{j,k} \equiv \langle \chi_j^I | \chi_k^I \rangle \quad (12)$$

$$(\mathbf{H}_{II'})_{j,k} \equiv \langle \chi_j^I | \hat{H}_{II'} | \chi_k^{I'} \rangle \quad (13)$$

$$(\dot{\mathbf{S}}_I)_{j,k} \equiv \langle \chi_j^I | \frac{\partial}{\partial t} | \chi_k^I \rangle \quad (14)$$

In the adiabatic representation, the electronic part of the Hamiltonian is diagonal (by definition) and so the only off-diagonal matrix elements of the total Hamiltonian are due to the nuclear kinetic energy operator. On the other hand, in the diabatic representation (used in the model study of bR described in this paper) the electronic basis is chosen so that the kinetic energy operator is diagonal (exactly or effectively) and it is the potential energy (*i.e.* the electronic Hamiltonian) that has off-diagonal matrix elements.

Having detailed the equations of motion for the electronic and nuclear degrees of freedom [eqn. (10) and (7)–(9), respectively] we now discuss the selection of basis functions representing population created after a non-adiabatic event. The dynamical expansion of the basis set (which we refer to as spawning) is one of the most important features of the method, governing both its numerical convergence and computational feasibility. Basis functions are spawned, *i.e.* added to the basis set, only during non-adiabatic events and, hence, we must first define a ‘non-adiabatic event.’ In the diabatic representation we define an effective non-adiabatic coupling strength for each basis function as

$$\mathbf{H}_{II'}^{\text{eff}}(\mathbf{R}) = \left| \frac{\langle I | \hat{H}_{II'} | I \rangle}{V_{I'}(\mathbf{R}) - V_I(\mathbf{R})} \right| \quad (15)$$

(see ref. 24 for the equivalent expression in the adiabatic representation). When the magnitude of the coupling strength for a given basis function exceeds a predetermined threshold, this basis function is considered to be in a non-adiabatic region. At this time, basis function must be introduced (*i.e.* spawned) on the coupled electronic state (I') which will represent the non-adiabatic population transfer. For problems of chemical interest, the regions of effective non-adiabatic coupling are, typically, spatially localized.^{42,43} By introducing the concept of a non-adiabatic event, unnecessary spawning attempts are avoided when the interstate coupling is negligible.

Once a basis function has entered a non-adiabatic region, it is propagated until the effective coupling falls below the spawning threshold in order to determine the ‘crossing time’, *i.e.* the time during which the effective non-adiabatic coupling exceeds the spawning threshold. The crossing time is divided into N_s equal intervals and within each of these intervals a basis function is spawned with zero population and with the same position as its parent. (Thus, N_s is the number of spawned basis functions per traversal of the non-adiabatic region.) The classical energy of the spawned basis function is required to be the same as that of its parent and, therefore, its momentum needs to be adjusted. Herman has shown that the best possible adjustment in the near-classical limit is along the non-adiabatic coupling vector,⁴⁴ a choice used previously by Tully on physical grounds.²⁶ Once the position and momentum of the newly spawned basis functions are known, they and the parent function are propagated backward in time to the beginning of the non-adiabatic event. At this point, the actual forward propagation continues, including the solution of the trajectory amplitudes for the newly spawned

basis function(s). The procedure that we use allows also for back-spawning, *i.e.* a newly populated electronic state is allowed to transfer population back to the other electronic state. Furthermore, we reject attempts to spawn basis functions that are redundant with other (occupied or unoccupied) basis functions on the same electronic state. By doing so we avoid the wasteful spawning of functions which, in any case, will be removed when the nuclear overlap matrix [\mathbf{S} in eqn. (10)] is inverted by a singular value decomposition procedure. In summary, the outlined procedure implies a forward propagation of a set of coupled electronic and nuclear equations of motion which is interrupted whenever a basis function enters a non-adiabatic region. At this point the above-described forward propagation, spawning and backward propagation is performed.

Many technical details, such as the specific choice of the various parameters that govern the numerical convergence of the method, as well as the initial values of the electronic and nuclear parameters that specify the initial wavefunction, are discussed in the next section.

Method

PESs

The three PESs used to model the photoisomerization of bR differ only in their dependence on one torsional coordinate: the angle ϕ about the $C_{13}=C_{14}$ double bond. The model treats the crossing between the 13-*cis* and the all-*trans* states as an avoided crossing, rather than a true one, *i.e.* a conical intersection.^{45,46} Proper accounting of conical intersections requires that the PESs of the coupled electronic states differ in at least two coordinates, for example the $C_{13}=C_{14}$ torsion and bond stretching. The functional form of the ϕ -dependent diabatic PESs (see Fig. 3) and of the ϕ -independent non-adiabatic coupling constants was chosen such that their diagonalized form (in the adiabatic representation) approximates the *ab initio* surfaces of the S_0 , S_1 and S_2 states in a retinal analogue $[\text{CH}_2-(\text{CH})_3-(\text{C}_2\text{H}_3)-(\text{CH})_2-\text{NH}-\text{CH}_3]^+$. We have also required that the vertical excitation energy $S_0 \rightarrow S_1$ be in agreement with the known excitation energy in retinal (50 kcal mol⁻¹).² The magnitude of the constant non-adiabatic potential-energy coupling terms V_{12} , V_{13} and V_{23} (the indices 1, 2 and 3 refer to the 13-*cis*, all-*trans* and singly excited states, respectively, see Fig. 3) were set to 0.5, 1 and 1 kcal mol⁻¹, respectively. This is considerably lower than would be estimated from the splitting in the *ab initio* PESs. However, *ab initio* prediction of energy gaps at avoided crossings can be very sensitive to the level of theoretical sophistication. Furthermore, previous simulations of the photoisomerization process with (mean-field) density matrix evolution methods^{17,18} showed that the quoted values resulted in a quantum yield that was in good agreement with the experimentally observed one (0.64).⁴⁷⁻⁵⁰

Molecular dynamics

At each point in time, the FMS method requires positions, momenta and forces for all the atoms as well as the nuclear phase according to eqn. (7)–(9) in order to build up the multi-dimensional time-dependent nuclear wavefunction. The method further requires that the forward and backward propagation of basis functions through the non-adiabatic region be time-reversible on the timescale of the non-adiabatic event, requiring the use of a small time step (1 fs). Hamilton's equations of motion were propagated using the velocity form of the Verlet integrator⁵¹ in a standard molecular dynamics scheme.

The simulations started with the refined bR₅₆₈ structure reported in ref. 11, which is based on a structure of bR obtained by electron microscopy.⁷ The structure of the retinal binding site is similar to the more recent structures obtained by electron

microscopy^{8,10} and X-ray crystallography.⁹ The refined bR structure was equilibrated for 15–20 ps and configurations were randomly selected as the initial structures for the simulation runs. The RMSDs between the chosen initial conditions are *ca.* 1 Å, on average.

The simulations were carried out in vacuum at 300 K, with a uniform relative permittivity of 1 and a 14 Å cut-off for Coulomb forces. The charmm19 force field and parameters⁵² were employed for all atoms except retinal, where a set of parameters calculated using *ab initio* quantum chemistry was employed.¹⁸

FMS method

Since the FMS method is derived from a variational principle it must converge to the numerically exact quantum-mechanical results, provided enough basis functions are used. In the case of bR, all 3762 atoms are explicitly included in the simulations (*i.e.* the multi-dimensional nuclear wavefunction in eqn. (5) was written as a product of $3 \times 3762 = 11286$ one-dimensional Gaussian functions). Thus, it is computationally impractical to ensure convergence with respect to all the parameters that define the time-dependent basis set and govern its size.

The same width parameter, $\alpha_{\rho_j}^I$, was used for all the coordinates on all three surfaces and its value was set to $10 a_0^{-2}$. This value is consistent with typical values obtained for C–C and C–H bonds in the harmonic approximation (where the natural choice for the width is related to mass and frequency⁴¹). Test simulations including only the retinal backbone showed that the branching ratio is insensitive to the width parameter for choices in the range 8–14 a_0^{-2} . These test simulations were also used to determine the magnitude of the effective non-adiabatic coupling [eqn. (15)] that triggers spawning. By running a few sample trajectories, and examining the magnitude of the effective non-adiabatic coupling as a function of time, we found that a threshold value of 0.5 is appropriate. This does not miss any of the non-adiabatic events which are usually indicated by ‘spikes’ in the effective coupling.²⁴ The number of spawned basis functions per traversal of the non-adiabatic region, N_s , was set to one. This value is too small to ensure that the fine details of the population transfer, as a function of time, are converged. From our previous experience, N_s should be set to 3 or more in order to ensure this. In previous studies, we have found that final branching ratios are within 5% of their converged values with $N_s = 1$.

We assume that only the singly excited electronic state (see Fig. 3) is initially populated. The initial state is modelled as a stationary state using a linear combination of sixteen uncorrelated nuclear basis states. Each of these states is parametrized by a single classical trajectory. (The equilibration procedure used to generate the initial conditions for the uncorrelated classical trajectories was discussed in the previous sub-section.) The initial amplitude of each basis function is set to unity and the trajectories are propagated sequentially. In principle, in order to model the dynamics of the initial nuclear wavefunction correctly, all the trajectories should be followed simultaneously thereby allowing the amplitudes to be coupled *via* the intrastate term H_{II} in eqn. (10). Given the short propagation time to the non-adiabatic region and the fact that the basis functions are not correlated (*i.e.* at $t = 0$ the overlap between any two nuclear basis functions is zero), the importance of these intrastate interferences for such a large system is not yet clear. In what follows we refer to each of the 16 trajectories as a ‘run’ and we discuss expectation values for both single runs and for the ensemble of 16 runs. Each of the 16 runs typically spawns 10 additional trajectories/basis functions.

A split-operator procedure⁵³ was used to propagate the set of coupled nuclear and electronic equations of motion [eqn. (7)–(9) and (10), respectively] in the diabatic representation. This approximation avoids the need to evaluate the diagonal matrix elements of the Hamiltonian [H_{II} in eqn. (10)] and the time derivative of the nuclear overlap

matrix [\hat{S}_I in eqn. (10)]. Since the diabatic potentials are coupled by a constant potential-energy coupling term, we were able to evaluate the off-diagonal matrix elements of the Hamiltonian [$H_{II'}$ in eqn. (10)] analytically. The electronic amplitudes (magnitude and phase) of the three electronic states and various (electronic state projected) nuclear observables, that we deem important for understanding the dynamics, were monitored as a function of time. Since the results are averaged over only a small number (16) of runs we centre our discussion on single runs and not on averaged results.

Results

Following optical excitation from the ground state all-*trans* PES to the singly excited state surface, retinal rotates around its $C_{13}=C_{14}$ bond. The time evolution of the population on one of the product states, the 13-*cis* state, is shown in Fig. 4. The spawning procedure that we employ results in a smooth population transfer, both for single runs and for the averaged results. We find that, although most of the population transfer occurs on a timescale of 300 fs, some population transfer occurs on a longer timescale, occasionally extending well beyond 1 ps (not shown). The final value of the population on the 13-*cis* electronic state, *i.e.* the photoisomerization quantum yield, is 48%. Considering the uncertainty in the electronic coupling between the all-*trans* and 13-*cis* electronic states and the statistical error due to our limited sample of 16 initial states, this value is in reasonable accord with the experimentally observed quantum yield of 0.64 ± 0.04 .⁴⁷⁻⁵⁰ The final value of the population on the all-*trans* electronic state is less than 1% (not shown). However, this result may be biased because we do not allow for a true crossing, *i.e.* a conical intersection, at the second crossing event, but rather model it as an avoided crossing (see Fig. 3).

As expected, the averaging procedure washes out some of the dynamical details of the population transfer which are observed in single runs (full and dashed thin lines in Fig. 4). Whereas the average population transfer is rather smooth, single runs show significant structure in the time dependence of the population transfer. The most prominent feature of the single runs is the, often observed, significant back transfer. Because the back transfer may (and does) occur at different time periods in different runs, only traces of it are observed in the averaged results and even these traces may be washed out upon averaging over a larger ensemble of runs. Since, in different runs, both the begin-

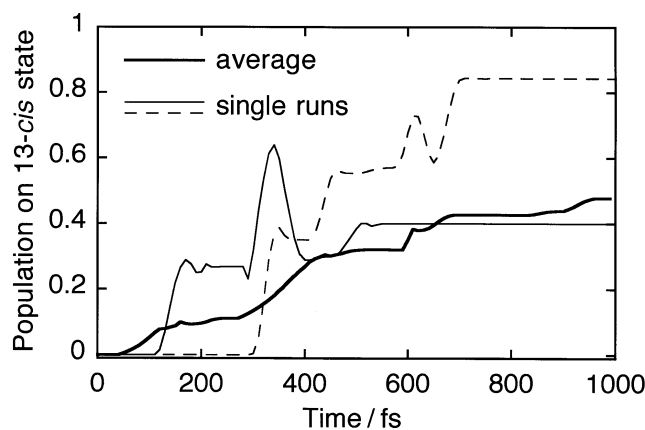


Fig. 4 Population on the 13-*cis* electronic state as a function of time. (—) Average result; (—) and (---) dashed lines: two typical single runs. Note that, whereas the average population transfer increases monotonically, significant back transfer is observed in single runs.

ning of the population transfer and its duration are quite different, the average duration of the population transfer is much longer than would be expected from the results of a single initial condition.

Before we proceed to discuss other expectation values, such as the torsion around the $C_{13}=C_{14}$ bond, it is instructive to distinguish between different isomerization pathways and products thereof. The all-*trans* \rightarrow 13-*cis* photoisomerization may proceed either clockwise or counter-clockwise, *i.e.* the Schiff base may rotate in the direction of Asp85 or in the direction of Asp212 (see Fig. 2). In either case, the isomerization products may assume two distinct structures. The Schiff base $N-H^+$ bond [which in the initial state is pointing toward the extracellular side (see Fig. 1)] may be oriented toward the cytoplasmic side of the protein or it may point approximately parallel to the plane of the membrane dividing cytoplasmic and extracellular spaces (see Fig. 5). If the isomerization proceeds *via* rotation in the direction of Asp85 and the latter structure is formed, then the $N-H^+$ bond remains connected to Asp85 *via* a hydrogen bond with an intermediate water molecule. Since, in a single run, the FMS method generates a wavefunction, which is represented as a linear superposition of basis functions parametrized using classical trajectories, the dynamics observed is quite rich and care must be taken in analysing the results. For example, we find that different basis functions (during the same simulation) may sometimes behave very differently. In such a case, the total wavefunction is delocalized and expectation values computed using this delocalized total wavefunction do not provide much useful dynamical information. Hence, in what follows, we discuss expectation values computed using the total wavefunction; yet, when required, we also discuss the behaviour of single basis functions. Because the final electronic population on the all-*trans* electronic state is negligible, we limit our discussion to expectation values on the singly excited and 13-*cis* electronic states.

All four of the above described scenarios, *i.e.* rotation toward the Asp85 or Asp212 with the Schiff base pointing up or sideways in the photoisomerization products, were observed in the ensemble of runs. Rotation in the Asp212 direction was less common than in the Asp85 direction. In the rare cases where the Schiff base rotated in the Asp212 direction and pointed sideways in the photoproduct, a hydrogen bond linking the Schiff base and water molecule 'W_A' was observed (see Fig. 2 and Fig. 6). In these cases, the Schiff base 'drags' water molecule W_A, *i.e.* the water molecule which bridges the Schiff base and Asp212, with it during the photoisomerization. Since this scenario was very uncommon we chose not to show it, but rather focus on more typical isomerization routes.

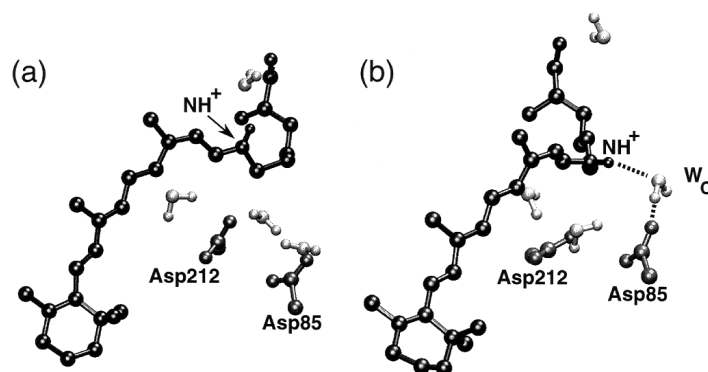


Fig. 5 (a) Photoisomerization product case 1 for which the retinal Schiff base proton points to Asp96. (b) Photoisomerization product case 2 for which the retinal Schiff base proton points to water, W_C, which forms a hydrogen bond with Asp85. This figure was created with VMD.⁵⁸

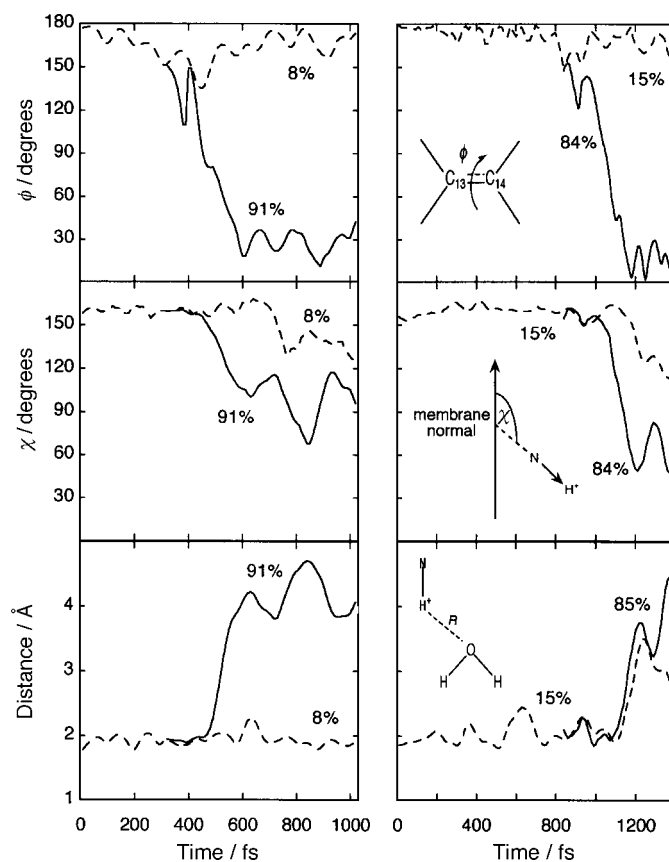


Fig. 6 Expectation values on the singly excited electronic state (---) and on the product 13-*cis* electronic state as a function of time (in fs). Upper panels: the $C_{13}=C_{14}$ torsion angle. Middle panels: the angle between the $N-H^+$ bond and a vector pointing along the membrane normal. Lower panels: the distance from the Schiff base proton to the oxygen atom of water molecule W_A . The results are for two single runs and the final population on each electronic state is indicated in each panel.

The two panels in Fig. 6 present typical examples for runs in which the isomerization proceeds in the Asp85 direction. In both panels we show expectation values on both the initially populated electronic state (dashed line) and on the product 13-*cis* electronic state (full line). The final population on each electronic state is indicated in the figure. The expectation value of the $C_{13}=C_{14}$ torsion angle as a function of time is shown in the uppermost right and left panels. Following excitation from the ground all-*trans* state to the singly excited state, retinal rotates around its $C_{13}=C_{14}$ bond until it approaches the first non-adiabatic region (the singly excited and 13-*cis* electronic states cross at an angle of 150° , see Fig. 3). Since there is a slight barrier *en route* to the curve-crossing region, the non-adiabatic events begin at different times (300 *vs.* 800 fs) in the two runs (right and left panels). (The beginning of the non-adiabatic event is indicated by the first point in time where the expectation value on the 13-*cis* state is shown.) At early times, when the wavefunction is in the non-adiabatic region ($\phi \approx 150^\circ$), the magnitude of the torsion angle on both electronic states is very similar, yet at the end of the photoisomerization process it is very different: the singly excited state remains in a *trans*-configuration ($\phi \approx 180^\circ$) whereas, on the 13-*cis* electronic state, the torsion angle librates

about 0° with an amplitude of *ca.* $20\text{--}40^\circ$. In both runs, the duration of the photoisomerization process is $250\text{--}300$ fs. As retinal rotates about the $C_{13}=C_{14}$ bond the orientation of the Schiff base $N-H^+$ bond varies. The angle between this bond and a vector pointing along the membrane normal is shown in the middle panels of Fig. 6. In the initial singly excited state, the Schiff base $N-H^+$ bond is pointing 'down', *i.e.* toward the extracellular side of bR (dashed lines in right and left middle panels). The middle right panel shows a case where the $N-H^+$ bond is oriented toward the cytoplasmic side of the protein (*i.e.* up) in the photoproduct. In contrast, the case depicted in the middle left panel ends with the $N-H^+$ bond oriented 'sideways', *i.e.* parallel to the plane of the membrane. In this latter case the Schiff base is connected to Asp85 *via* a hydrogen bond with an intermediate water molecule. As the Schiff base is rotating, the hydrogen bond between the Schiff base proton and water molecule W_A is broken (lower right and left panels). This water molecule remains bound to the Schiff base proton on the singly excited state whereas, on the *13-cis* state, this bond is broken quite rapidly, within 200 fs.

Finally, we discuss an interesting run that results in isomerization in both the Asp85 and Asp212 directions. The upper panel in Fig. 7 shows the expectation value of the torsion angle as a function of time on the singly excited state (dashed line) and on the product *13-cis* state (full line). As in Fig. 6, the final population on these two electronic

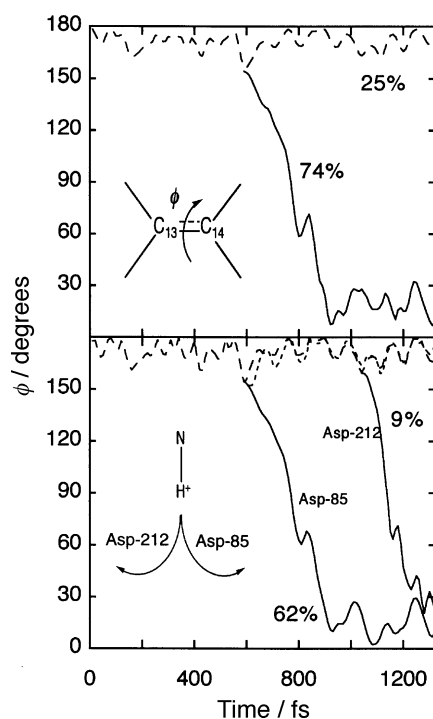


Fig. 7 Upper panel: expectation value of the $C_{13}=C_{14}$ torsion angle as a function of time (in fs) on the singly excited electronic state (---) and on the product *13-cis* electronic state (—). The results (in both panels) are for a single run and the final population on each electronic state is indicated in the panel. Lower panel: same as upper panel, but for four basis functions carrying most of the population (the final population of the basis functions associated with the *13-cis* state is indicated in the panel). (---) Basis functions associated with the singly excited electronic state; (—) basis functions associated with the *13-cis* electronic state. The basis function that ends with 62% of the population rotates toward Asp85, whereas the one that ends with 9% of the population rotates toward Asp212.

states is indicated. The trajectories travelled by four basis functions carrying most of the population (the final populations of the basis functions associated with the 13-*cis* state are indicated in the figure) are shown in the lower panel of Fig. 7. As in the upper panel, dashed lines are used for basis functions on the singly excited state and full lines are used for basis functions on the product 13-*cis* state. The average expectation values shown in the upper panel of Fig. 7 are quite similar to those shown in the upper (right and left) panels of Fig. 6: the torsion angle isomerizes on the 13-*cis* state in *ca.* 300 fs. However, the details of this run, shown in the lower panel, are much more revealing. The initially populated basis function (travelling on the singly excited electronic state) spawns a basis function on the 13-*cis* electronic state at $t = 600$ fs. Shortly after this basis function is spawned, it ‘back-spawns’ a basis function on the singly excited state. This basis function, that is propagating on the singly excited state, spawns a basis function on the 13-*cis* state at much later time, $t = 1$ ps. The two basis functions travelling on the 13-*cis* state isomerize on similar timescales, yet *via* two different pathways: in the first basis function (which carries 62% of the population) the Schiff base rotates toward Asp85 whereas, in the second basis function, (which carries 9% of the population) it rotates toward Asp212. Both basis functions travelling on the 13-*cis* electronic state end with the Schiff base N—H⁺ bond pointing up toward the cytoplasmic side of the protein (not shown).

Discussion

The results of this study again exemplify the important role of molecular dynamics simulations in extending investigations on proteins to a level of detail which is beyond experimental resolution, and crucial for an understanding of the mechanisms of protein function.⁶ An entirely quantum-mechanical description of sub-picosecond protein dynamics has been accomplished on a heuristic potential surface which allows for at least three qualitatively different reaction pathways. Because of the involvement of several electronic states, the use of quantum dynamics is essential. Such description is possible for a large system like bR because of the FMS method.^{22,24,25} The FMS method capitalizes on the strength of classical mechanics in selecting the regions of Hilbert space which are most relevant to the ensuing non-adiabatic wave packet dynamics. The analogy to classical mechanics has permitted the use of an existing, albeit modified, molecular dynamics program.^{54,55} The successful application of the method suggests its use in future studies of elementary reactions in proteins.

This study focused specifically on the primary photoreaction of bR which involves a femtosecond photoisomerization of the protein’s retinal chromophore. In this first application of quantum dynamics to protein photocycles, only a small number of simulations could be carried out. Nevertheless, there arose a rich set of isomerization scenarios with compelling suggestions regarding bR’s function. In agreement with previous classical⁶ and combined classical/quantum-mechanical molecular dynamics studies,¹⁸ we report here a sub-picosecond timescale for the key primary processes, torsion around retinal’s C₁₃=C₁₄ bond and non-adiabatic crossings. The simulations also revealed the occurrence of two types of photoisomerization products. These had been previously identified with a putative precursor for the pump process and with a side product which could be of possible functional significance, *e.g.* in the case of an overcharged bacterial membrane.^{6,56}

Our study also provides significant differences to previous investigations. The present simulations do not exhibit any slowing near the potential crossing at a 90° torsion of the C₁₃=C₁₄ bond, avoiding, thereby, any chance for crossing back to the all-*trans* state on the sub-picosecond timescale. However, the results above suggest that, after 1 ps, 52% of the optically excited retinal remains in the excited state, while the balance isomerizes to a 13-*cis* conformation. The ultimate fate of the long-lived excited-

state population cannot be stated on the basis of the simulations presented here. Nevertheless, one anticipates that energy redistribution will lead to a damping of the torsional energy. This may lead to a much more equitable branching between *cis* and *trans* products arising from the long-lived population, as compared to the population which undergoes prompt internal conversion.

Most intriguing in regard to functional implications is the observation that photoisomerization occurs in two opposite rotational senses and that the direction of rotation is correlated with the formation of different photoproducts. It appears that one rotational sense leads predominantly to a product (case II) which is likely to trigger proton pumping, whereas the other rotational sense leads to a product (case I) which has been implicated with a reversal of proton pumping as it arises in certain mutants and, possibly, in the presence of electric fields under intense radiation.^{56,57}

The present investigation is likely to be considerably extended in the future. Foremost is a need to improve the potential surfaces of retinal. In particular, one should include the effect of electronic excitation on other degrees of freedom. For example, accounting for the weakened force constant of the C₁₃=C₁₄ stretching motion in the excited state may lead to an energetically accessible conical intersection. This could have a profound effect on the photodynamics, since internal conversion is known to be extremely efficient when conical intersections are encountered. Another improvement which is needed is the recognition of the differing charge distributions and polarizabilities of the electronic states. This may be especially important in the light of the importance of nearby ionized residues, as elucidated by metagenesis studies. A second great opportunity for further advances arises through the availability of much improved structures of bR. The observed structures will likely need to be completed through placement of internal waters, which can play a crucial role and need to be represented faithfully.

The proton pump function of bR was discovered more than 20 years ago and, so far, has escaped explanation, despite a barrage of investigations. The resolution of the structure of bR in combination with quantum-mechanical descriptions of the photoprocess may soon provide the long sought after explanation.

The authors thank W. Humphrey for fruitful discussions. This work was supported by the National Institutes of Health (NIH PHS 5 P41 RR05969), by the National Science Foundation (NSF BIR 94-23827 EQ, NSF/GCAG BIR 93-18159, MAC93S028 NSF-CHE-97-33403), and by the Roy J. Carver Charitable Trust. T.J.M. thanks Research Corporation and the National Science Foundation (for Research Innovation and CAREER awards, respectively).

References

- 1 R. H. Lozier, R. A. Bogomolni and W. Stoeckenius, *Biophys. J.*, 1975, **15**, 955.
- 2 R. A. Mathies, S. W. Lin, J. B. Ames and W. T. Pollard, *Annu. Rev. Biochem. Biophys.*, 1991, **20**, 491.
- 3 J. K. Lanyi, *J. Bioenerg. Biomemb.*, 1992, **24**, 169.
- 4 D. Oesterhelt, J. Tittor and E. Bamberg, *J. Bioenerg. Biomemb.*, 1992, **24**, 181.
- 5 T. Ebrey, in *Thermodynamics of Membranes, Receptors and Channels*, ed. M. Jacobson, CRC Press, New York, 1993, p. 353.
- 6 K. Schulten, W. Humphrey, I. Logunov, M. Sheves and D. Xu, *Israel J. Chem.*, 1995, **35**, 447.
- 7 R. Henderson, J. M. Baldwin, T. A. Ceska, F. Zemlin, E. Beckmann and K. H. Downing, *J. Mol. Biol.*, 1990, **213**, 899.
- 8 N. Grigorieff, T. Ceska, D. Downing, J. Baldwin and R. Henderson, *J. Mol. Biol.*, 1996, **259**, 393.
- 9 E. Pebay-Peyroula, G. Rummel, J. Rosenbusch and E. Landau, *Science*, 1997, **277**, 1676.
- 10 Y. Kimura, D. Vassilyev, A. Miyazawa, A. Kidera, M. Matsushima, K. Mitsuoka, K. Murata, T. Hirai and Y. Fujiyoshi, *Nature (London)*, 1997, **389**, 206.
- 11 W. Humphrey, I. Logunov, K. Schulten and M. Sheves, *Biochemistry*, 1994, **33**, 3668.
- 12 D. Xu, C. Martin and K. Schulten, *Biophys. J.*, 1996, **70**, 453.
- 13 S. J. Doig, P. J. Reid and R. A. Mathies, *J. Phys. Chem.*, 1991, **95**, 6372.

- 14 B. S. Hudson, B. E. Kohler and K. Schulten, in *Excited States*, ed. E. C. Lim, Academic Press, New York, 1982, vol. 6, p.1.
- 15 P. Tavan and K. Schulten, *Phys. Rev. B*, 1987, **36**, 4337.
- 16 K. Schulten, U. Dinur, and B. Honig, *J. Chem. Phys.*, 1980, **73**, 3927.
- 17 J. Mavri, H. J. C. Berendsen and W. F. V. Gunsteren, *J. Phys. Chem.*, 1993, **97**, 13469.
- 18 W. Humphrey, H. Lu, I. Logunov, H. J. Werner and K. Schulten, to be published.
- 19 U. Genick, G. Borgstahl, K. Ng, Z. Ren, C. Pradervand, P. Burke, V. Srajer, T-T. Teng, W. Schildkamp, D. McRee, K. Moffat and E. Getzoff, *Science*, 1997, **275**, 1471.
- 20 R. Kosloff, *Annu. Rev. Phys. Chem.*, 1994, **45**, 145.
- 21 T. J. Martínez, M. Ben-Nun and G. J. Ashkenazi, *J. Chem. Phys.*, 1996, **104**, 2847.
- 22 T. J. Martínez, M. Ben-Nun and R. D. Levine, *J. Phys. Chem.*, 1996, **100**, 7884.
- 23 M. Ben-Nun, T. J. Martínez and R. D. Levine, *J. Phys. Chem. A*, 1997, **101**, 7522.
- 24 T. J. Martínez, M. Ben-Nun and R. D. Levine, *J. Phys. Chem. A*, 1997, **101**, 6389.
- 25 M. Ben-Nun and T. J. Martínez, *J. Chem. Phys.*, 1998, **108**, 7244.
- 26 J. C. Tully and R. K. Preston, *J. Chem. Phys.*, 1971, **55**, 562.
- 27 J. C. Tully, *J. Chem. Phys.*, 1990, **93**, 1061.
- 28 N. C. Blais and D. G. Truhlar, *J. Chem. Phys.*, 1983, **79**, 1334.
- 29 P. Pechukas, *Phys. Rev.*, 1969, **181**, 174.
- 30 F. J. Webster, P. J. Rossky and R. A. Friesner, *Comput. Phys. Commun.*, 1991, **63**, 494.
- 31 F. J. Webster, E. T. Wang, P. J. Rossky and R. A. Friesner, *J. Phys. Chem.*, 1994, **104**, 4835.
- 32 G. D. Billing, *Int. Rev. Phys. Chem.*, 1994, **13**, 309.
- 33 H. D. Meyer and W. H. Miller, *J. Chem. Phys.*, 1979, **70**, 3214.
- 34 H. D. Meyer and W. H. Miller, *J. Chem. Phys.*, 1980, **72**, 2272.
- 35 M. Ben-Nun, T. J. Martínez and R. D. Levine, *Chem. Phys. Lett.*, 1997, **279**, 319.
- 36 T. J. Martínez, *Chem. Phys. Lett.*, 1997, **272**, 139.
- 37 T. J. Martínez and R. D. Levine, *J. Chem. Phys.*, 1996, **105**, 6334.
- 38 T. J. Martínez and R. D. Levine, *Chem. Phys. Lett.*, 1996, **259**, 252.
- 39 M. Ben-Nun and R. D. Levine, *Chem. Phys.*, 1995, **201**, 163.
- 40 M. Ben-Nun, R. D. Levine and G. R. Fleming, *J. Chem. Phys.*, 1996, **105**, 3035.
- 41 E. J. Heller, *J. Chem. Phys.*, 1975, **62**, 1544.
- 42 M. Klessinger and J. Michl, *Excited States and Photochemistry of Organic Molecules*, VCH, New York, 1995.
- 43 D. R. Yarkony, *J. Chem. Phys.*, 1996, **100**, 18612.
- 44 M. F. Herman, *J. Chem. Phys.*, 1984, **81**, 754.
- 45 V. Bonacic-Koutecky, K. Schoffel and J. Michl, *Theoret. Chim. Acta*, 1987, **72**, 459.
- 46 M. Garavelli, P. Celani, F. Bernardi, M. A. Robb and M. J. Olivucci, *J. Am. Chem. Soc.*, 1997, **119**, 6891.
- 47 G. Schneider, R. Diller and M. Stockburger, *Chem. Phys.*, 1989, **131**, 17.
- 48 R. Govindjee, S. P. Balashov and T. G. Ebrey, *Biophys. J.*, 1990, **58**, 597.
- 49 S. Logunov, M. El-Sayed and L. Song, *J. Phys. Chem.*, 1996, **100**, 2391.
- 50 S. Logunov, M. El-Sayed and J. Lanyi, *Biophys. J.*, 1996, **70**, 2875.
- 51 W. C. Swope, H. C. Andersen, P. H. Berens and K. R. Wilson, *J. Chem. Phys.*, 1982, **76**, 637.
- 52 B. R. Brooks, R. E. Bruccoleri, B. D. Olafson, D. J. States, S. Swaminathan and M. Karplus, *J. Comput. Chem.*, 1983, **4**, 187.
- 53 T. J. Martínez and R. D. Levine, *J. Chem. Soc., Faraday Trans.*, 1997, **93**, 940.
- 54 M. Nelson, W. Humphrey, A. Gursoy, A. Dalke, L. Kalé, R. D. Skeel and K. Schulten, *J. Supercomputing App.*, 1996, **10**, 251.
- 55 J. C. Phillips, R. Brunner, A. Shinozaki, M. Bhandarkar, N. Krawetz, L. Kalé, R. D. Skeel and K. Schulten, in *Algorithms for Macromolecular Modelling*, ed. P. Deuffhard, J. Hermans, B. Leimkuhler, A. Mark, R. D. Skeel and S. Reich, Lecture Notes in Computational Science and Engineering, Springer-Verlag, in press.
- 56 W. Humphrey, E. Bamberg and K. Schulten, *Biophys. J.*, 1997, **72**, 1347.
- 57 G. Nagel, B. Kelety, B. Mockel, G. Buldt and E. Bomberg, *Biophys. J.*, 1998, **74**, 403.
- 58 W. F. Humphrey, A. Dalke and K. Schulten, *J. Mol. Graphics*, 1996, **14**, 33.